Short communication

Estimation of the kinetic parameters of processes at the negative plate of lead-acid batteries by impedance studies

S.M. Rezaei Niya*, M. Hejabi, F. Gobal

Department of Chemistry, Sharif University of Technology, P.O. Box 11365-9516, Tehran, Iran

ARTICLE INFO

ABSTRACT

Impedance characteristics of the negative electrode of lead-acid battery were derived on the basis of fundamental interfacial processes occurring at the electrode. The solution of the governing equations was presented in terms of a simple equivalent circuit consisting of resistive and capacitive loops in which charge transfer and sulfate layer formation and also mass transfer (Warburg) elements are considered. The kinetic parameters were deduced by fitting the theoretically derived impedance to the experimental data. Impedance at various States of Charge (SoC) was also examined.

© 2010 Elsevier B.V. All rights reserved.

1. Introduction

With the increasing demand of automotive industry to more robust and reliable power sources, battery modeling, monitoring and management play ever more significant roles (e.g., Refs. [1–5]). There are different batteries' modeling methods with different capabilities depending on the number of governing equations and parameters employed. Computational Fluid Dynamics (CFD) methods are usually efficient to solve large sets of nonlinear differential equations for modeling battery operations. However, many of the parameters have to be determined through extensive kinetics and thermodynamics measurements that render the method incapable of management and control of the dynamic behavior of batteries (e.g., Refs. [6–9]). The methods based on the use of artificial neural networks can only make predictions in the domain of the data used to train the networks and lack extrapolation capabilities [10,11]. The success of the modeling methods of equivalent circuit, which approximate battery's components (also operation) by electrical circuits, depends on how correctly both qualitatively and quantitatively the allocations are made (e.g., Refs. [12–14]). The method of electrochemical impedance spectroscopy (EIS) is capable of correlating and identifying the equivalent circuit components with the actual physical chemistry of the battery's components and processes proceeding in the electrodes and battery. Interestingly,

the batteries can be analyzed under vastly different conditions and States of Charge (SoC) (e.g., Refs. [15–21]) using this technique. In principle, all the kinetic parameters (charge transfer, mass transfer) can be determined [22,23]. The method has successfully been applied to model the positive electrode of lead-acid battery [22]. The purpose of the present work was to combine EIS measurements and the electrochemical mechanisms of the charge–discharge processes of negative electrode aiming at finding the correlation between the equivalent circuit model of the system's electrochemistry inside the battery and the results of EIS measurements largely manifested in the Nyquist plots.

2. Methods

The overall charge–discharge process occurring at the negative electrode of a lead-acid battery is given as
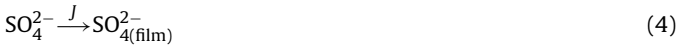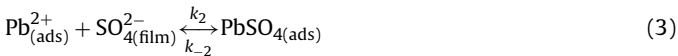
$$Pb + HSO_4^- \Leftrightarrow PbSO_4 + H^+ + 2e^- \quad E^\circ = -0.340\,V \quad (1)$$
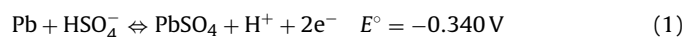
It is believed that in the discharge process, $PbSO_4$ nuclei forms and the three-dimensional growth continue through the electrodissolution of Pb and the incorporation of Pb^{2+} species into the growing nuclei assisted by HSO_4^-. The three-dimensional growth continues until the entire surface of the electrodes is covered by a layer of $PbSO_4$ through that the transport of SO_4^{2-} is responsible for further growth of the thickness of the layers. The sequence of the explained events probably occurs at low and high anodic overpotentials [24,25]. The discharge process can be further presented

in more details as

$$Pb \underset{k_{-1}}{\overset{k_1}{\longleftrightarrow}} Pb^{2+}_{(ads)} + 2e^- \tag{2}$$

$$Pb^{2+}_{(ads)} + SO^{2-}_{4(film)} \underset{k_{-2}}{\overset{k_2}{\longleftrightarrow}} PbSO_{4(ads)} \tag{3}$$

$$SO^{2-}_4 \overset{J}{\longrightarrow} SO^{2-}_{4(film)} \tag{4}$$

where Pb^{2+} ions formed electrochemically react with the diffusing SO_4^{2-} to form the growing lead sulfate layer. The modeling of the mechanism starts with expressing the charge transfer rate as [26]:

$$i = \vec{i} - \overleftarrow{i} = nF\left[k_1(1-\theta)\exp\left(-\frac{\alpha nF\varphi}{RT}\right) - k_{-1}\theta\exp\left(\frac{\beta nF\varphi}{RT}\right)\right] \tag{5}$$

where θ, φ, α and β are the surface coverage of adsorbed lead ion, polarization potential and symmetry factors for the reduction and oxidation processes, respectively and temperature (T) is set at 300 K. Under the impedance measurement regime:

$$i = \bar{i} + \tilde{i}, \quad \theta = \bar{\theta} + \tilde{\theta}, \quad \varphi = \bar{\varphi} + \tilde{\varphi} \tag{6}$$

where barred symbols are steady state and tilde symbols signify the frequency dependent quantities generally expressed as:

$$\tilde{B} = B_0 \exp(j\omega t) \tag{7}$$

with B_0 being the amplitude of these variables, ω and t, are the angular velocity of the signal and time, respectively and j is $\sqrt{-1}$.

The time derivative of Eq. (5) is then:

$$\frac{d\tilde{i}}{dt} = \left[\frac{-\vec{i}}{1-\theta} - \frac{\overleftarrow{i}}{\theta}\right]\frac{d\tilde{\theta}}{dt} + \left[\frac{-\alpha nF}{RT}\vec{i} - \frac{\beta nF}{RT}\overleftarrow{i}\right]\frac{d\tilde{\varphi}}{dt} \tag{8}$$

and thus:

$$\tilde{i} = \left[\frac{-\vec{i}}{1-\theta} - \frac{\overleftarrow{i}}{\theta}\right]\tilde{\theta} + \left[\frac{-\alpha nF}{RT}\vec{i} - \frac{\beta nF}{RT}\overleftarrow{i}\right]\tilde{\varphi} \tag{9}$$

The interfacial impedance is by definition:

$$Z = -\frac{\tilde{\varphi}}{\tilde{i}} \tag{10}$$

which can be broken down into two parts:

$$Z = Z_f + Z_h \tag{11}$$

with

$$Z_f = \frac{RT}{nF(\alpha\vec{i} + \beta\overleftarrow{i})} = \frac{RT}{nFi_0} = R_{ct} \tag{12}$$

and

$$Z_h = \left[\frac{RT}{nF(\alpha\vec{i} + \beta\overleftarrow{i})} \frac{\theta\vec{i} + (1-\theta)\overleftarrow{i}}{\theta(1-\theta)}\right]\frac{\tilde{\theta}}{\tilde{i}} \tag{13}$$

The first (i.e., Eq. (12)) is the charge transfer impedance (resistance) and the second (i.e., Eq. (13)) is the impedance due to SO_4^{2-} diffusion and adsorption of Pb^{2+}. Assuming the prevalence of equilibrium (that is the measurements were carried out at open circuit potential), θ is found to be

$$\theta = \frac{k_1}{k_1 + k_{-1}\exp(nF\varphi/RT)} \tag{14}$$

with $K = k_{-1}/k_1$ and $a = \exp(nF\varphi/RT)$.

Substituting in Eq. (12) and (13) one has:

$$R_{ct} = \frac{RT}{nFi_o} = \frac{RT}{n^2F^2k_1\exp(-\alpha nF\varphi/RT)} \times \frac{1+Ka}{Ka} \tag{15}$$

$$Z_h = \frac{RT}{nF\bar{\theta}(1-\bar{\theta})}\frac{\tilde{\theta}}{\tilde{i}} = \frac{RT}{nF}\frac{(1+Ka)^2}{Ka}\frac{\tilde{\theta}}{\tilde{i}} \tag{16}$$

To find $\tilde{\theta}/\tilde{i}$, precipitation reaction, Eq. (3), is considered. Assuming first order kinetics [26], one has:

$$\frac{d[Pb^{2+}]}{dt} = \frac{i}{nF} - k_2[Pb^{2+}]\left[SO_4^{2-}\right] + k_{-2}[PbSO_4] \tag{17}$$

Defining Γ as the maximum coverage attained by lead sulfate and considering the θ definition:

$$\Gamma\frac{d\theta}{dt} = \frac{i}{nF} - k_2\Gamma\theta x_{SO_4^{2-}} + k_{-2}(1-\theta)\Gamma \tag{18}$$

where $x_{SO_4^{2-}}$ is the surface concentration of SO_4^{2-} ions at the film surface. If this is not dramatically perturbed by the applied ac signal, by separating the alternate parts and dc parts it can be obtained:

$$\Gamma\frac{d\bar{\theta}}{dt} = \frac{\bar{i}}{nF} - k_2\Gamma\bar{\theta}\bar{x}_{SO_4^{2-}} + k_{-2}(1-\bar{\theta})\Gamma \tag{19}$$

$$nF\Gamma\frac{d\tilde{\theta}}{dt} = \tilde{i} - nFk_2\Gamma\left(\tilde{\theta}\bar{x}_{SO_4^{2-}} + \bar{\theta}\tilde{x}_{SO_4^{2-}}\right) - nFk_{-2}\tilde{\theta}\Gamma \tag{20}$$

In dc parts equation (i.e., Eq. (19)), because of equilibrium, $\bar{i} = 0$ and $d\bar{\theta}/dt = 0$, so

$$\bar{x}_{SO_4^{2-}} = \frac{k_{-2}(1-\bar{\theta})}{k_2\bar{\theta}} \tag{21}$$

In alternate parts equation (i.e., Eq. (20)), because of Eq. (7), $d\tilde{\theta}/dt = j\omega\tilde{\theta}$. Using Eq. (21) one arrives at

$$nF\Gamma j\omega\tilde{\theta} = \tilde{i} - nFk_2\Gamma\left(\tilde{\theta}\frac{k_{-2}(1-\bar{\theta})}{k_2\bar{\theta}} + \bar{\theta}\tilde{x}_{SO_4^{2-}}\right) - nFk_{-2}\Gamma\tilde{\theta} \tag{22}$$

Substituting the surface concentration of SO_4^{2-} by its flux [21,27]:

$$\tilde{J} = \tilde{x}_{SO_4^{2-}}f(j\omega, D) \tag{23}$$

where $f(j\omega, D)$ depends on the electrode shape:

$$\tilde{i} = nF\Gamma j\omega\tilde{\theta} - nF\tilde{J} \tag{24}$$

and

$$\tilde{x}_{SO_4^{2-}} = \frac{nF\Gamma j\omega\tilde{\theta} - \tilde{i}}{nF\overleftrightarrow{f}(j\omega, D)} \tag{25}$$

For planar electrodes [27]:

$$f(j\omega, D) = \frac{\sqrt{j\omega D}}{\tanh[\delta\sqrt{j\omega/D}]} \tag{26}$$

So, Eq. (22) would be:

$$\frac{f(j\omega, D) + k_2\Gamma\bar{\theta}}{nF}\frac{\tilde{i}}{\tilde{\theta}} = \frac{j\omega\bar{\theta}f(j\omega, D) + \Gamma k_{-2}f(j\omega, D) + j\omega k_2\Gamma\bar{\theta}^2}{\bar{\theta}} \tag{27}$$

Using Eqs. (14), (16), and (27), finally one has

$$Z_h = \frac{RT(1+Ka)^2}{n^2F^2\Gamma Ka}$$
$$\times \frac{(1+Ka) + k_2\Gamma\tanh\left[\delta\sqrt{j\omega/D}\right]/\sqrt{j\omega D}}{(1+Ka)j\omega + k_{-2}(1+Ka)^2 + k_2\Gamma j\omega\tanh\left[\delta\sqrt{j\omega/D}\right]/\sqrt{j\omega D}} \tag{28}$$

Adding the double layer capacitance, C_{dl}, and the solution ohmic resistance, R_s, the overall equivalent circuit representing the negative electrode of lead-acid battery is finally represented in Fig. 1. The circuit elements, extracted from Eq. (28) are

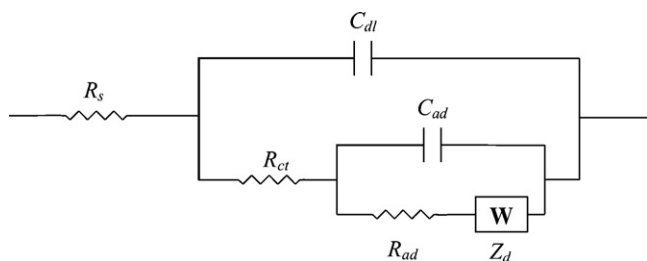$$R_{ct} = \frac{RT\exp(\alpha nF\varphi/RT)(1+Ka)}{An^2F^2k_1Ka} \tag{29}$$

Fig. 1. The equivalent circuit of negative electrode.

$$C_{ad} = \frac{A\Gamma n^2 F^2 Ka}{RT(1 + Ka)^2} \qquad (30)$$

$$R_{ad} = \leftrightharpoons \frac{RT(1 + Ka)}{An^2 F^2 Ka\Gamma k_{-2}} \qquad (31)$$

$$Z_d = \frac{RTk_2}{An^2 F^2 Kak_{-2}} \tanh\left[\delta\sqrt{j\omega/D}\right] / \sqrt{j\omega D} \qquad (32)$$

and C_{dl} takes the usual form [26]:

$$C_{dl} = \left(\frac{2n^2 F^2 \varepsilon\varepsilon_0 n^0}{NRT}\right)^{1/2} \cosh\left(\frac{nF\varphi}{2RT}\right) \times A \qquad (33)$$

where $\varepsilon, \varepsilon_0$ and n^0 are the relative dielectric constant of the medium (electrolyte), permittivity of vacuum, the bulk concentration of the ions forming the double layer structure, respectively.

3. Materials and experimental methods

A two-electrode cell consisting of a negative plate and two inter-connected positive plates of 12SB3 motorcycle MF batteries was assembled. Each electrode had dimensions of 70.00 mm × 45.00 mm × 2.02 mm and separated by Adsorbed Glass Matt (AGM). A 4.5 M (1.28 s g) sulfuric acid solution was used as the electrolyte. The electrochemically active area of the negative plate was 10.7 m^2 as measured by impedance spectroscopy using charge transfer resistance, double layer charging, electrolyte resistance and governing equations for porosity [31]. The surface area was estimated from the pore volume. It was supposed that the pores are full spheres [28].

Impedance measurements were carried out using electrochemical system comprising of a Solartron 1470 Electrochemical Interface and Solartron 1260A Impedance Analyzer where frequency range of 10 kHz to 10 mHz and ac signal amplitude (amplitude of the modulation signal) of 10 mV were employed. Studies were carried out at open circuit potential [29] with the electrode being at various States of Charge (SoC) in the range of 10–100%. To further validate the results, negative electrode having dimensions of 35.00 mm × 45.00 mm × 2.02 mm with the surface area of 4.73 m^2 was also studied.

4. Results and discussions

Fig. 2 presents the Nyquist plot of electrodes where similar patterns have been observed. The Nyquist plots consist of two overlapping semi-circles at the high and medium frequency regions terminating to a virtually straight line at the low frequency end of the spectrum. This trend is also reported by others (i.e., Ref. [30]). The repeatability and the consistency of the results are good, as shown in Fig. 2. Fig. 3 presents a comparison between the experimental and numerical data for the 10.7 m^2 and 4.73 m^2 electrochemically active area plates. As can be seen in Eqs. (29)–(33), there are unknown parameters that should be estimated based on experimental results (like $k_1, k_{-1}, k_2, k_{-2}, \ldots$). Therefore in first
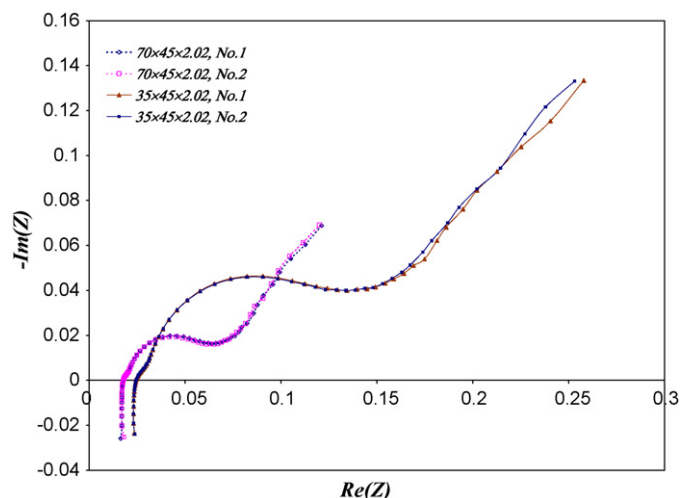

Fig. 2. The area dependency and repeatability of Nyquist plots for negative plates.

step, the experimental results of 10.7 m^2 electrochemically active area plate (larger plate) were used to estimate these values. Table 1 presents the values of the kinetic parameters obtained through the one to one correspondence of the theory and the experimental findings. The larger plate plot reveals that with a proper choice of the kinetic parameters, the numerical model seems to reproduce the experimental trend. In next step, the same kinetic parameters were used to model 4.73 m^2 electrochemically active area plate (smaller plate). As can be seen in Fig. 3, the theoretical results are in excellent agreement with their counterpart experimental data. The Nyquist plots consist of basically three frequency regions, excluding the frequencies above 500 Hz where the response of the measuring instrument is affected by the connecting wirings, etc. [31]. In the frequency regions of 500–40 Hz the appearance of a semi-circle seems to be due to the combination of C_{dl} and R_{ct}. These elements in turn depend on the kinetic parameters of the charge transfer reaction ($k_1, k_{-1}, \ldots$) and the relevant double layer capacitor (ε & n^0). Substituting the relevant values for a (1.58×10^{-17} at the measurement potential) and neglecting Ka (as it is much less than unity) the charge transfer resistance would be simply dependent just on the reciprocal of k_{-1}. So, one can find k_{-1} by fitting this semi-circle in numerical model and experimental results. The second semi-circle in the frequency range of 40–0.5 Hz signifies the impedance of the adsorbed layer. The size of this semi-circle is thus related to R_{ad} and C_{ad} and therefore to relevant kinetic parameters as well as
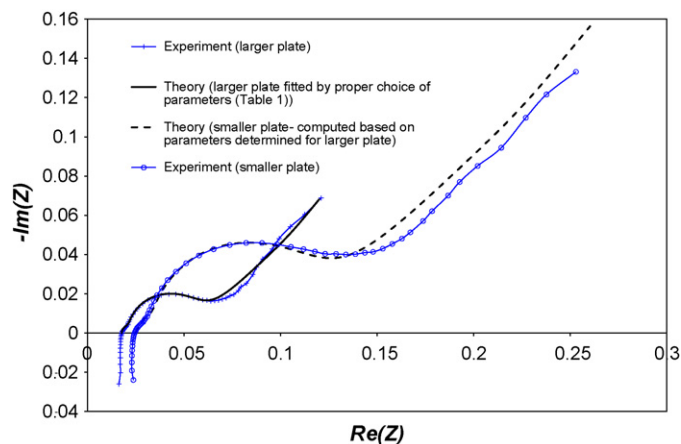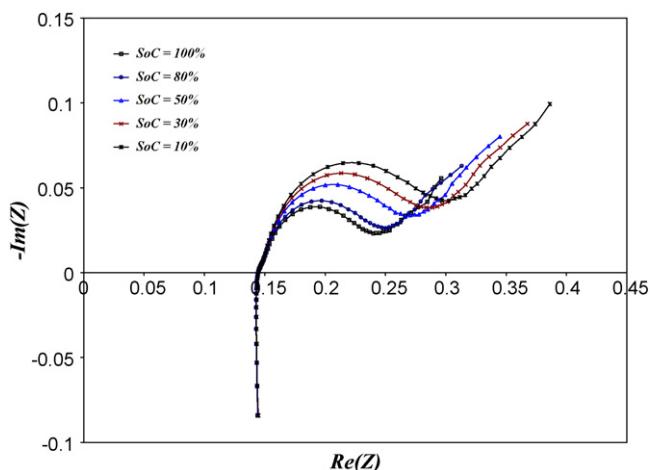

Fig. 3. The Nyquist plot comparison of procured equivalent circuit and experimental data for both plates.

Table 1
Supposed values for kinetic parameters.

	Parameters					
	k_1 (mol m^{-2} s^{-1})	k_{-1} (mol m^{-2} s^{-1})	k_2 (m^2 mol^{-1} s^{-1})	k_{-2} (s^{-1})	Γ (mol m^{-2})	D (m^2 s^{-1})
Values	78e−3	218	934e−12	444	1e+5	102e−11

Table 2
Values of equivalent circuit elements for two plates.

	R_{ct}	C_{dl}	R_{ad}	C_{ad}	$Z_d \times \sqrt{j\omega D}/\tanh(\delta\sqrt{j\omega/D})$
Larger plate	0.0072	2.73	0.0318	7.08	2.97e−8
Smaller plate	0.0163	1.21	0.0719	3.13	6.71e−8

Fig. 4. Experimental evaluation of SoC variation effect on Nyquist plots.

Fig. 6. The Nyquist plot dependency of model to rate constant of dissolution reaction variations (k_{-2}).

Γ. The virtually straight line appearing in the frequency domain of 500–10 mHz signifies the mass transfer control processes occurring at the electrolyte–electrode interface. The slope of the line is nearly unity and it is indeed so-called Warburg impedance. Hence, other kinetic parameters can be estimated by fitting the adsorbed layer semi-circle and mass transfer straight line in numerical model and experimental results.

The magnitudes of the equivalent circuit elements are provided in Table 2. Fig. 4 presents the experimental Nyquist plots recorded at various States of Charge. Decreasing the States of Charge results in higher impedance of the interface (lower metallic character or higher lead sulfate thickness) as expected while the charge trans-

fer process is least affected. To further amplify the usefulness of the model, various Γ's, maximum lead contents, which corresponds to various SoC's, were fed into Eqs. (30) and (31) and Nyquist plots were calculated. The trend shown by the modeling results presented in Fig. 5 is in good agreement with that of the experimental data shown in Fig. 4.
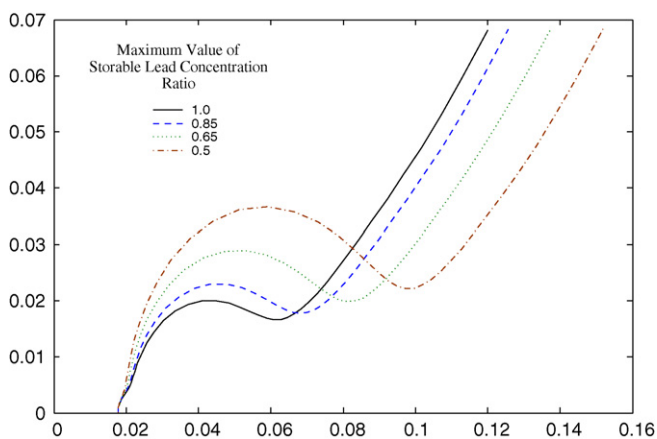
Fig. 6 presents the changes of the Nyquist plot brought about by various k_{-2} values. It seems that an accurate combination of maximum value of storable lead concentration (Γ) (Fig. 5) and rate constant of dissolution reaction (k_{-2}) (Fig. 6) can predict state of Charge (SoC) (Fig. 4) precisely.

5. Conclusion

Theoretical derivation of the interfacial impedance of the electrolyte/negative plate of lead-acid batteries, equivalent circuit model and experimental determination of the interfacial impedance characteristics were combined to derive the kinetics and diffusional parameter of the processes of charge/discharge at this electrode. In practice, three frequency regions signifying charge transfer, formation of lead sulfate and diffusion through the lead sulfate layer are observed. Kinetics and mass transfer parameters are reported.

Fig. 5. The Nyquist plot dependency of model to maximum value of storable lead concentration (Γ) variations.

References

[1] D.A.J. Rand, P.T. Moseley, Valve-Regulated Lead Acid Batteries, Elsevier, USA, 2004.
[2] M. Shiomi, T. Funato, J. Power Sources 64 (1997) 147–152.
[3] P.E. Pascoe, A.H. Anbuky, Energ. Convers. Manage. 45 (2004) 1015–1041.
[4] E. Meissner, G. Richter, J. Power Sources 95 (2001) 13–23.
[5] T. Okashi, K. Yamada, T. Hirasawa, A. Emori, J. Power Sources 158 (2006) 874–878.
[6] W.B. Gu, G.C. Wang, C.Y. Wang, J. Power Sources 108 (2002) 174.

[7] V. Srinivasan, G.Q. Wang, C.Y. Wang, J. Electrochem. Soc. 150 (2003) 316–325.
[8] H. Gu, T.V. Nguyen, J. Electrochem. Soc. 12 (1987) 134.
[9] W.B. Gu, C.Y. Wang, B.Y. Liaw, J. Electrochem. Soc. 144 (1997) 2053–2061.
[10] W.X. Shen, Energ. Convers. Manage. 48 (2007) 433–442.
[11] W.X. Shen, C.C. Chan, E.W.C. Lo, K.T. Chau, Energ. Convers. Manage. 43 (2002) 817–826.
[12] Y. Guo, M. Wu, S. Mua, J. Power Sources 64 (1997) 65–69.
[13] C. Rerolle, R. Wiart, Electrochem. Acta 40 (1995) 939–948.
[14] E. Karden, S. Buller, J. Power Sources 85 (2000) 72–78.
[15] S.R. Nelatury, P. Singh, J. Power Sources 112 (2002) 621–625.
[16] S.R. Nelatury, P. Singh, J. Power Sources 132 (2004) 309–314.
[17] M. Thele, O. Bohlen, D.U. Sauer, E. Karden, J. Power Sources 175 (2008) 635–643.
[18] S. Buller, M. Thele, E. Karden, J. Power Sources 113 (2002) 422–430.
[19] A.J. Salkind, A. Cannone, J. Power Sources 116 (2003) 174–184.
[20] M. Thele, E. Karden, E. Surewaard, D.U. Sauer, J. Power Sources 158 (2006) 953–963.
[21] C. Wang, J. Electrochem. Soc. 145 (1998) 1801–1812.
[22] M. Hejabi, A. Oweisi, N. Gharib, J. Power Sources 158 (2006) 944–948.
[23] S.D. McAllister, R. Ponraj, I.F. Cheng, D.B. Edward, J. Power Sources 173 (2007) 882–886.
[24] M. Thele, J. Schiffer, E. Karden, E. Surewaad, D.U. Sauer, J. Power Sources 168 (2007) 31–39.
[25] J.R. Viche, F.E. Varela, J. Power Sources 64 (1997) 39–45.
[26] A.J. Bard, L.R. Faulkner, Electrochemical Methods: Fundamentals and Applications, 2nd ed., John Wiley & Sons, USA, 2001.
[27] T. Jacobsen, K. West, Electrochem. Acta 40 (1995) 255–262.
[28] M. Hejabi, S.M. Rezaei Niya, Proceeding of 7th Biennial Electrochemistry Seminar of Iran (7 BESI), August 28–30, 2007, p. 138.
[29] M.P. Vinod, K. Vijayamohanan, J. Power Sources 52 (1994) 135–139.
[30] C.V. D'Alkaine, P. Mengarda, P.R. Impinnisi, J. Power Sources 191 (2009) 28–35.
[31] K.V. Rybalka, L.A. Beketaeva, J. Power Sources 30 (1990) 269–273.